

Effects of cutting parameters on dry cutting of aluminum bronze alloy

Shengguan Qu · Fujian Sun · Liang Zhang ·
Xiaoqiang Li

Received: 21 April 2013 / Accepted: 5 September 2013 / Published online: 22 September 2013
© Springer-Verlag London 2013

Abstract High-strength wear-resisting aluminum bronze alloy is a difficult-to-machine material. Dry cutting tests were conducted on high-strength wear-resisting aluminum bronze alloy with YW1 cemented carbide tool and YBC251 coated cemented carbide tool. The wear mechanisms of the two tools were characterized with a scanning electron microscope (SEM) and an energy-dispersive spectrometer (EDS) to compare their machining performances. And on that basis, the influences of cutting parameters, including cutting speed, feed rate, and cutting depth, on the tool life of the YBC251 coated cemented carbide tool and surface roughness of the workpiece were analyzed with a 3-D super-depth-of-field instrument and a surface profile measuring instrument, respectively. The results showed that the machining performance of the YBC251 coated cemented carbide tool was better than that of the YW1 cemented carbide tool. Among all the cutting parameters, it was found that feed rate had a stronger effect on tool life and surface roughness than cutting speed and cutting depth.

Keywords Cemented carbide tool · High-strength wear-resisting aluminum bronze alloy · Wear mechanism · Tool life · Surface roughness

1 Introduction

Aluminum bronzes are copper-base alloys containing approximately 5 to 12 wt% Al. Major alloying elements other than Al include Fe, Ni, Mn, and Si [1]. And it is well known that

aluminum bronze has excellent physical, mechanical, and tribological properties; shows excellent sliding wear resistance against steel; and possesses very good corrosion resistance in neutral saline and even low-concentration H_2SO_4 solution [2–5]. That outstanding property makes the material extraordinarily useful in the machine building industry; for example, with the remarkable wear resistance, aluminum bronze is employed for stretching and squeezing dies [6] and for aluminum bronze coating of cutting tools [7]. However, these properties also result in the tendency to be machined with mechanical methods with a very big difficulty [6].

Based upon considering the comprehensive properties of aluminum-bronze alloy and design principles of the micro-structure of aluminum-bronze alloy, Li et al. [1] developed a new high-strength and wear-resisting aluminum bronze. Compared with the Japanese AIBC2(JIS H5114-79) and the French U-A9Fe3Y200(NFA 53-709-70), its yield strength was 44.5 and 19.7 % higher, and its Brinell hardness was 16.6 and 11.9 % higher, respectively [1]. The machinability of the high-strength wear-resisting aluminum bronze was explored with the M2 high-speed steel tool and YW1 cemented carbide tool, and the machining performance of the M2 tool was confirmed to be worse than that of the YW1 tool under the experimental condition [8, 9].

In the present paper, in order to further study the machinability of the high-strength wear-resisting aluminum bronze, two kinds of cutting tools, YW1 cemented carbide tool and YBC251 coated cemented carbide tool, are utilized to cut the aluminum bronze, the wear mechanisms of the two kinds of cutting tools are studied and compared, and the influences of cutting parameters on both tool life of YBC251 coated cemented carbide tool and surface roughness of the workpiece are also studied in the cutting process.

S. Qu (✉) · F. Sun (✉) · L. Zhang · X. Li
School of Mechanical and Automotive Engineering, South China
University of Technology, Guangzhou 510640, China
e-mail: qusg@scut.edu.cn
e-mail: Lancesfj@126.com

Table 1 Chemical composition of workpiece material (in weight percent)

Al	Fe	Ni	Mn	Pb	Ti	B	Cu
9.0–10.5	3.0–5.0	1.0–2.5	1.0–2.5	≤1.0	≥0.5	≤0.2	Balanced

2 Experimental design

2.1 Experimental material

The chemical composition of the high-strength and wear-resistant aluminum bronze alloy developed by Li et al. [1] is shown in Table 1 [1], and its mechanical properties are shown in Table 2 [1]. YW1 cemented carbide tool and YBC251 coated (TiN/Al₂O₃/TiCN) cemented carbide tool, characterized by the tool angle parameters shown in Table 3, are used to cut a cylindrical bar of the workpiece material.

2.2 Experimental process

The cutting experiments were carried out on C6132A1 lathe shown in Fig. 1. Neither lubricant nor coolant was used in the cutting process. The cutting parameters of cutting speed 88 m/min, feed rate 0.1 mm/r, and cutting depth 2 mm were employed to study wear mechanisms, and the experiments were stopped at the cutting time of 5, 10, and 15 min to analyze the changing wear morphology with increasing cutting time. Panels a and b of Fig. 2 show the chips produced by YW1 cemented carbide tool and YBC251 coated cemented carbide tool, respectively. To explore the influences of cutting parameters on tool life, another series of experimental works were carried out with the cutting conditions of cutting speed 33–88 m/min, feed rate 0.05–0.21 mm/r, and cutting depth 0.4–1.2 mm. The influences of cutting parameters on surface roughness were also investigated over wide ranges of cutting speed from 8 to 176 m/min, feed rate from 0.05 to 0.34 mm/r, and cutting depth from 0.1 to 3.0 mm.

SEM photograph and surface chemical composition of a worn tool face were characterized with a scanning electron microscope and energy-dispersive spectrometer, respectively. The measurement of the wear band width of the tool flank was done with a 3-D super-depth-of-field instrument, and surface roughness was measured with a surface profile measuring instrument.

Table 2 Mechanical properties of workpiece material

Tensile strength (σ_b /MPa)	Yield strength ($\sigma_{0.2}$ /MPa)	Elongation (δ /%)	Brinell hardness (HB)	Impact toughness (α_k /J cm ⁻²)
633	370	18	169	43

Table 3 Tool parameters of YW1 cemented carbide tool and YBC251 coating cemented carbide tool

	Rake angle	Relief angle	Cutting edge angle	Minor edge angle
YW1	6°	6°	45°	45°
YBC251	6°	6°	95°	5°

3 Results and discussion

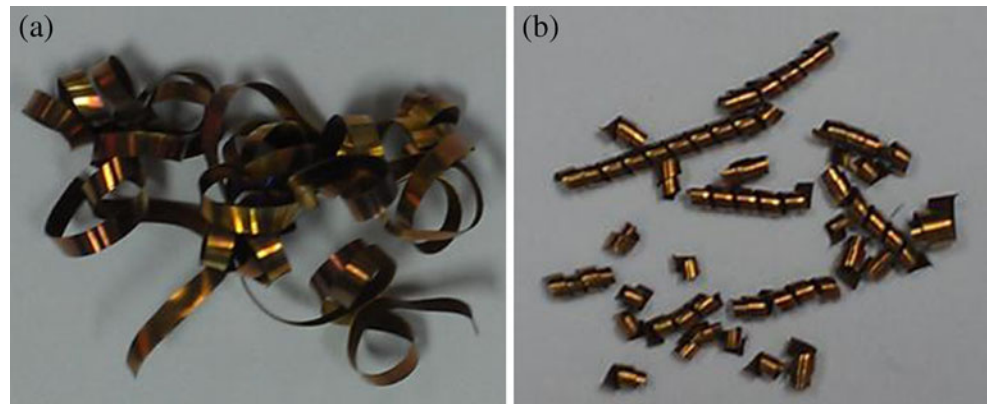
3.1 The wear of YW1 cemented carbide tool

Figures 3 and 4 show the SEM photographs of rake faces and flank faces of YW1 cemented carbide tool, respectively. It can be seen from Fig. 3a, b that an obvious crater does not form on the rake face, and a large area of a notch (Fig. 3a) appears on the cutting edge close to the nose, which is possibly caused by abrasive wear between solid particles of the tool material, such as tungsten carbide (WC) compound, and the workpiece material. A small amount of the adhesive forms as shown in Fig. 4b, which is likely to be aluminum–bronze alloy. And the tool substrate is obviously exposed (Fig. 4a). However, because the affinity of the WC compound of the cemented carbide tool to Cu and Al elements of the workpiece material is small and the hardness of the tool material is high, it is obvious that adhesive wear is not a main wear mechanism [9]. After machining for 10 min and even 5 min, micro-chipping appears on the rake face and flank face; 15 min of machining makes tool micro-chipping become so obvious that the tool loses its usability. So the failure mode of the YW1 cemented carbide tool is not tool flank wear, but micro-chipping.

To further study the wear mechanisms of the YW1 cemented carbide tool, a series of chemical composition analyses of the tool flank wear surface for 10 min of machining with EDS are shown in Table 4. In Table 4 (a), the main component is WC and there also exists a little amount of Co element from the binder of the tool material. Obviously, the chemical composition is close to that of the tool substrate. It

**Fig. 1** Domestic lathe C6321A1 for cutting experiment

Fig. 2 Chips produced by **a** YW1 cemented carbide tool and **b** YBC251 coated cemented carbide tool (cutting speed 88 m/min, feed rate 0.1 mm/r and cutting depth 2 mm)



demonstrates that the cemented carbide tool substrate has been exposed and that peeling wear is one of the wear mechanisms. In Table 4 (b), the dark area contains approximately 50 wt% C and 44 wt% O. In high temperature, C compounds of the tool decompose out the C element to diffuse into the workpiece; thus, on the tool surface, a concentration gradient of C element is formed to increase the C content of the tool surface [8]. And simultaneously, the diffusion reduces the content of C to degrade properties of the tool [10]. The O existence is attributed to the high cutting temperature. As a result, the high-temperature oxidation reactions of the C element diffused from the tool, and the metallic elements from the workpiece material, such as Al and Fe, react with oxygen in the air to generate the corresponding carbon oxygen compounds and metallic oxides. However, in the experiment by Li et al. [8], the oxidation reaction was not mentioned in the machining process of the aluminum bronze with the YW1 tool. The chemical composition in Table 4 (c) is basically the same as that of the aluminum bronze alloy. The phenomenon also demonstrates that adhesive wear appears in the tool surface.

3.2 The wear of YBC251 coated cemented carbide tool

Figure 5 shows the SEM photographs of rake faces of the YBC251 coated cemented carbide tool. There is no crate and

notch in the rake faces, maybe because the coating structure reduces the friction force between the tool and the workpiece, and improves the surface properties of the tool. However, in Fig. 5 (a and c), a little amount of layer material appears on the tool nose, and it is highly possible to be built-up edge, which is caused by the adhesive wear between the tool and the workpiece material.

Figure 6 shows the SEM photographs of flank faces of YBC251 coated cemented carbide tool. A wear band of about 0.12 mm in width is seen to form. This phenomenon is very normal for the cutting process, which is caused by the friction between flank face and workpiece material. The adhered aluminum bronze layer is found in the flank. During the cutting process, in the conditions of high cutting temperature and big cutting force, the workpiece material easily adheres to the cutting tool by the adsorption force between molecules. However, in the cutting process with the YBC251 coated cemented carbide tool, the tool surface roughness increases with the mutual friction between the workpiece and the tool. At the same time, the cutting temperature is very high in the cutting process with high cutting speed so as to decrease the hardness of the workpiece material and increase the plasticity. Therefore, the aluminum bronze alloy very easily fills in the tool surface micro-cavities and micro-grooves to protect the tool. Thus, it can be seen that the adhered workpiece material

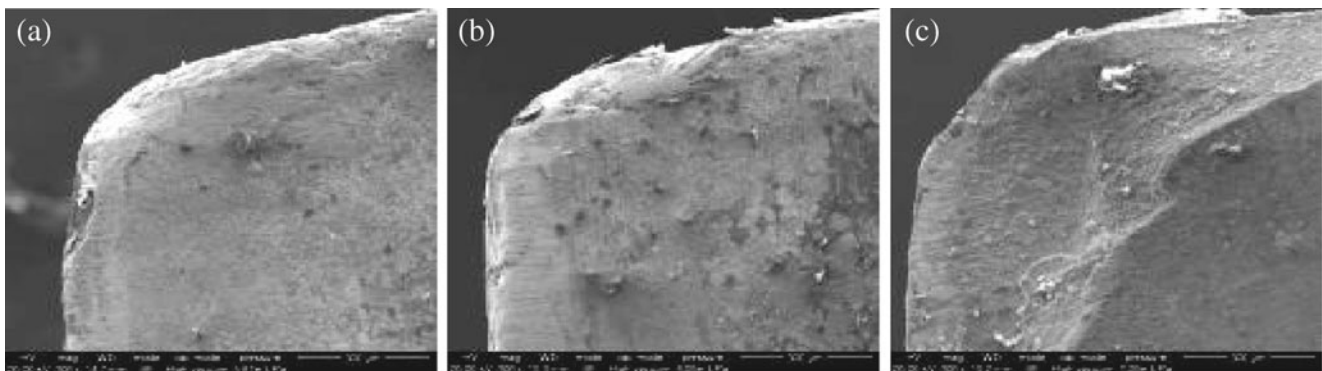


Fig. 3 SEM photographs of rake faces of YW1 cemented carbide tool. **a** 5, **b** 10, **c** 15 min

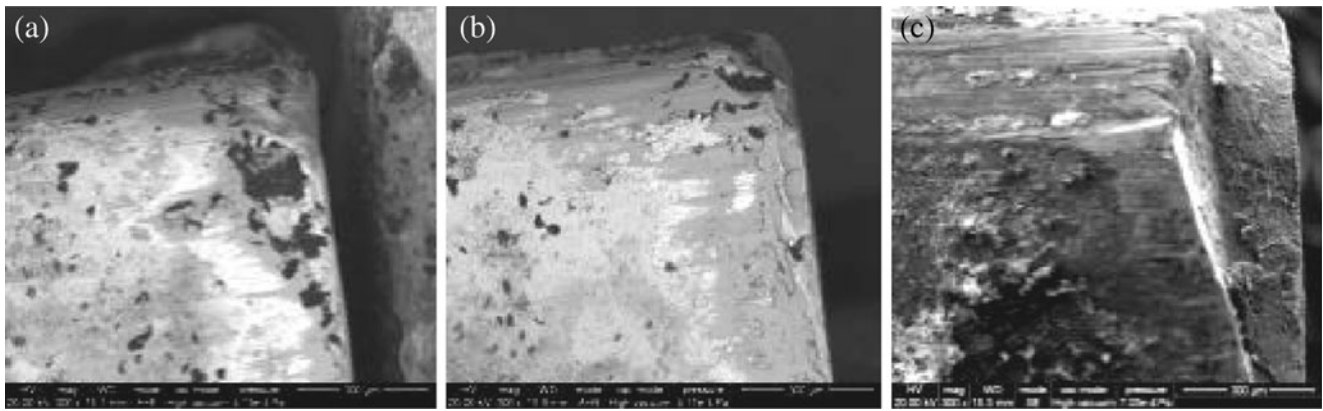


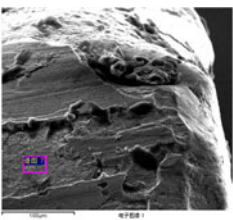
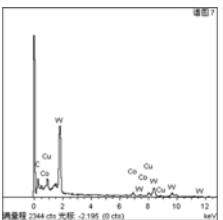
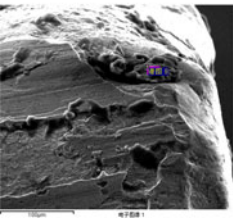
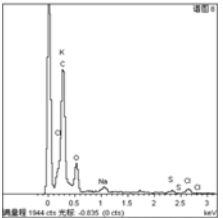
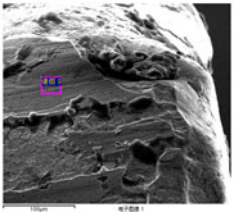
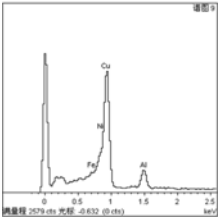
Fig. 4 SEM photographs of flank faces of YW1 cemented carbide tool. **a** 5, **b** 10, **c** 15 min

layer on the tool surface is related not just with adhesive wear, but also with the phenomenon of so-called smearing of tool flank [11]. Because of the high strength and the high hardness of YBC251 coated cemented carbide tool, tool flank does not form micro-chipping.

The SEM photographs and the chemical composition of the wear band for 10 min machining are showed in Table 5. Table 5 (a) shows that the chemical composition is very close to that of cemented carbide. And a little amount of Cu and Al elements come from the aluminum bronze. It can be

concluded that peeling wear is also one of the wear mechanisms of YBC251 coated cemented carbide tool. The chemical composition shown in Table 5 (b) is basically the same as that of the workpiece material except the Ti and Ni elements. Compared with 2.0 wt% Ti, only approximately 0.5 wt% Ti is contained in the aluminum bronze. The reason why the Ti concentration is much so high is a result of the coating material of the cutting tool. That phenomenon also proves that serious adhesive wear forms on the flank face. As shown in Table 5 (c), C and O elements constitute the main chemical

Table 4 Chemical composition analysis of the YW1 cemented carbide tool wear surface for 10 min of machining

Number	SEM photograph	Element mass percent	Energy spectrum
(a)		C: 11.93 % Co: 5.82 % Cu: 7.96 % W: 74.29 %	
(b)		C: 49.62 % O: 44.2 % Na: 1.8 % S: 0.82 % Cl: 1.51 % K: 1.25 %	
(c)		Al: 13.17 % Fe: 2.93 % Ni: 3.28 % Cu: 80.62 %	

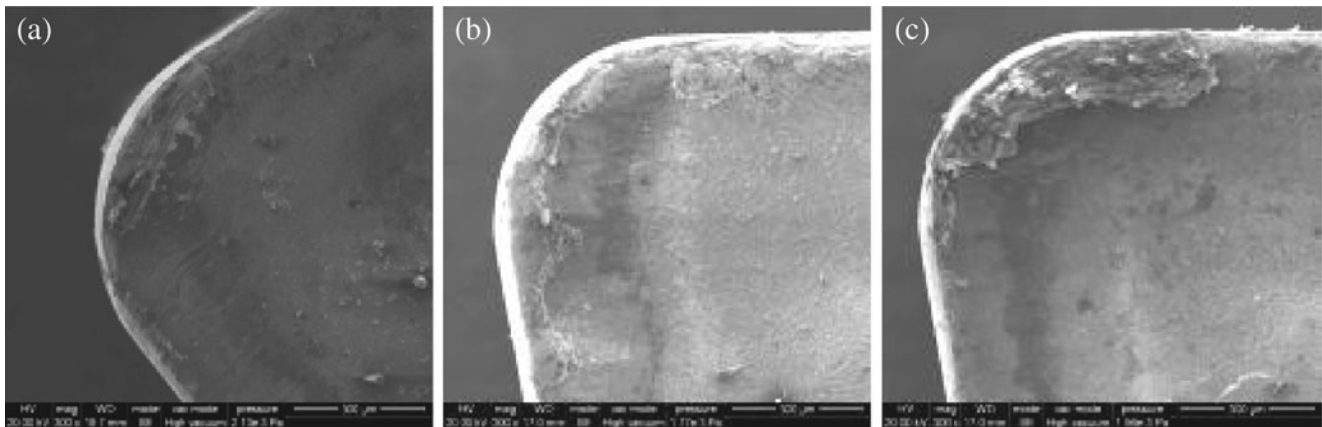


Fig. 5 SEM photographs of rake faces of YBC251 coated cemented carbide tool. **a** 5, **b** 10, **c** 15 min

elements. The forming mechanism is very similar with the forming mechanism described for Table 4 (b). However, the coating structure of YBC251 coated cemented carbide tool weakens carbon diffusion and oxidation reaction. From the above analysis, in the cutting process, the coating has been moved, and the coating failure exposes the cutting tool substrate. And it had been confirmed in ref. [12, 13] that although coating delamination had appeared in the initial machining process, the coating structure improved tool machining performance. And the coating delamination forms the smooth surface, which creates the opportunity to develop the adhered aluminum bronze layer. It is concluded that both delamination wear and adhesive wear appear in the flank wear band.

3.3 YBC251 coated cemented carbide tool life analysis

Under the actual working condition of cutting speed 88 m/min, feed rate 0.1 mm/r, and cutting depth 2.0 mm, the progression of tool flank wear band versus cutting time is characterized with a 3-D super-depth-of-field instrument shown in Fig. 7. With the increase of cutting time, the average wear band width of worn flank face VB gradually increases. The failure mode of YBC251 coated cemented carbide tool is average flank wear.

Figure 8 shows the progression of wear band widths VB versus cutting time. The average wear band width of flank wear VB of 0.3 mm was selected as the tool life rejection criterion of the coated cemented carbide tool. As seen in Fig. 8, the tool wear band width reaches 0.3 mm after 90-min cutting. Before the cutting time of 90 min, the cutting is in the normal wear stage, and after that time, the tool wear degree speeds up with the cutting time increasing; the cutting is into a serious wear stage. It is concluded that the tool life of YBC251 coated cemented carbide tool is 90 min under the actual working condition.

3.3.1 The influence of cutting speed

Figure 9 shows the evolution of tool wear progression versus cutting time under different cutting speeds. Before the cutting time of 15 min, the cutting process is in the initial wear stage; the tool wear band widths are almost constant for the different cutting speeds. After 15 min, the cutting process is in normal wear stage, and the tool wear degrees for the different cutting speeds are obviously different. And before the cutting time of 25 min, the VB for the cutting speed of 55 m/min is less than that for the cutting speeds of 33 and 88 m/min. The phenomenon should be explained in terms of the change of main tool

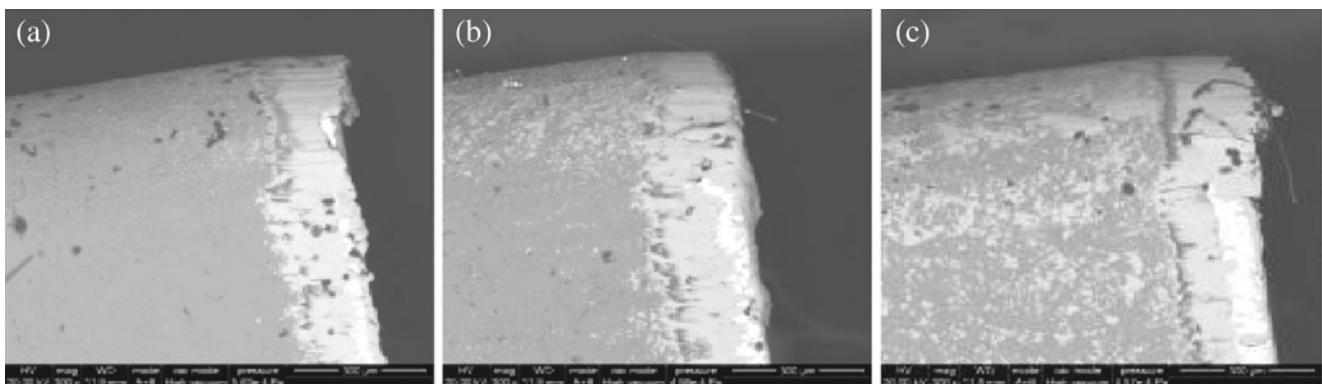
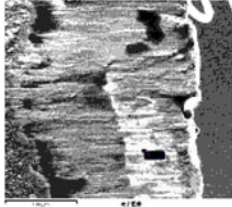
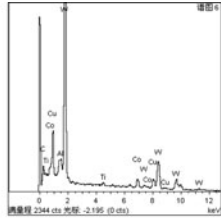
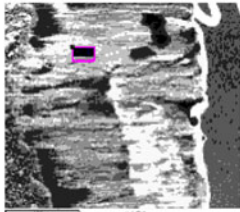
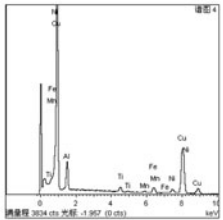
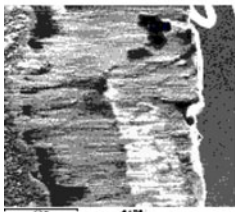
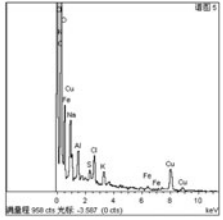
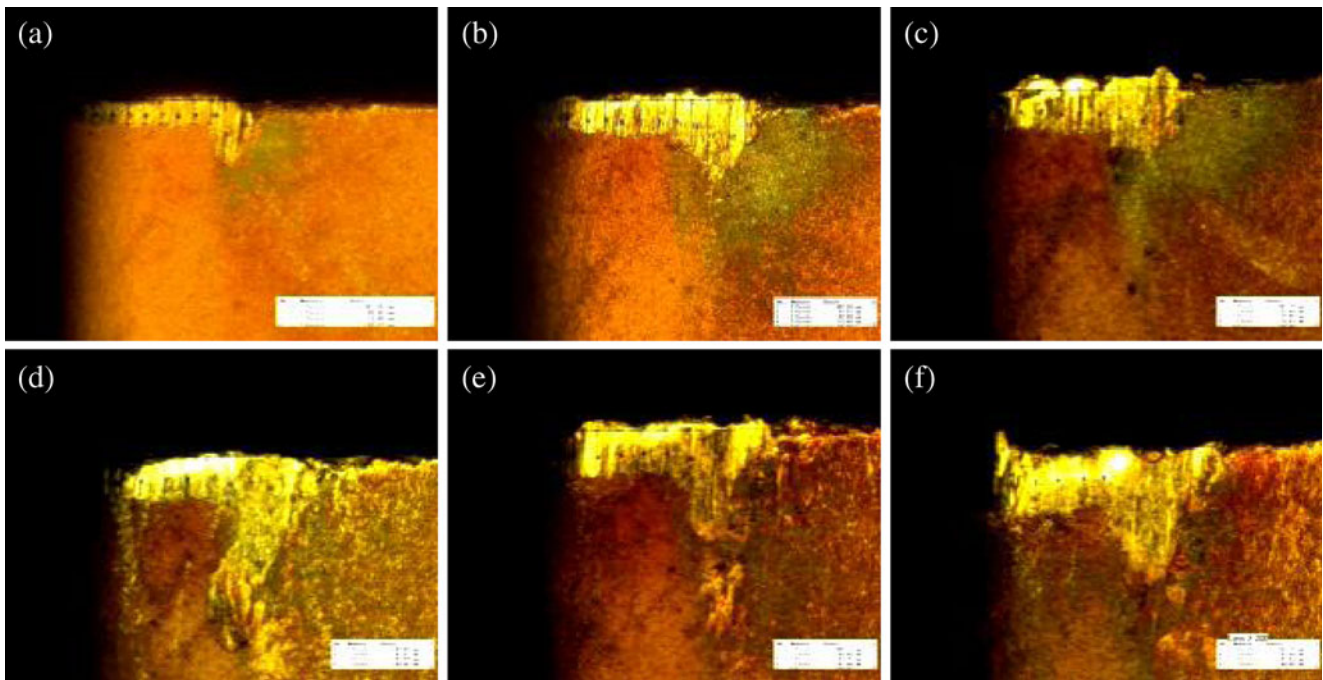


Fig. 6 SEM photographs of flank faces of YBC251 coating cemented carbide tool. **a** 5, **b** 10, **c** 15 min

Table 5 Chemical composition analysis of the wear band surface of the YBC251 coated cemented carbide tool for 10 min of machining

	SEM photograph	Element mass percent	Energy spectrum
(a)		C: 5.04 % Al: 1.59 % Ti: 1.04 % Co: 4.93 % Cu: 7.57 % W: 79.84 %	
(b)		Al: 12.64 % Ti: 2.22 % Mn: 0.89 % Fe: 4.05 % Ni: 4.19 % Cu: 76.01 %	
(c)		C: 46.58 % O: 29.98 % Na: 3.55 % Al: 2.16 % Cl: 2.26 % Cu: 1.46 %	

**Fig. 7** Progress of tool flank wear band of YBC251 coated cemented carbide tools versus cutting time (cutting speed 55 m/min, feed rate 0.1 mm/r, cutting depth 0.8 mm). **a** 5, **b** 10, **c** 15, **d** 20, **e** 25, **f** 30 min

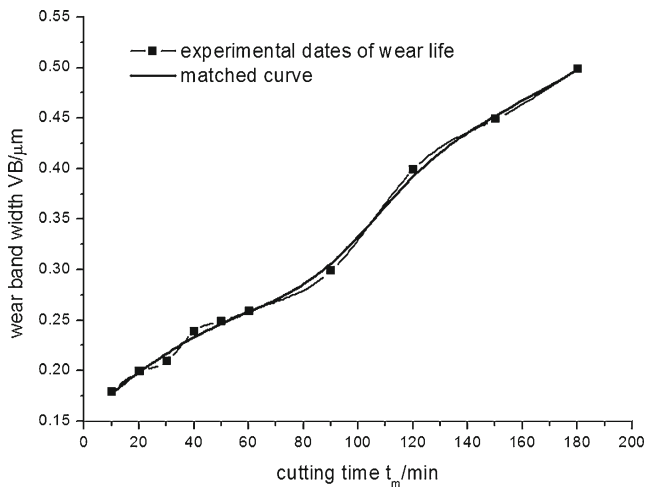


Fig. 8 Progress of VB versus cutting time (cutting speed 55 m/min, feed rate 0.1 mm/r, cutting depth 0.8 mm)

wear mechanisms with increasing cutting speeds. In the condition of low cutting speed, adhesive wear led by built-up edge is very serious. While for high cutting speed, the formation condition of the built-up edge weakens gradually, the main wear mechanism is therefore no longer the adhesive wear caused by the built-up edge [14]. At the same time, although chips carry off more heat in a high cutting speed, the cutting temperature still dramatically increases to intensify the adhesive and diffusive wear in the flank face. So it sharply increases the flank wear band width and reduces the tool life [13, 15, 16].

3.3.2 The influence of feed rate

Figure 10 shows the progression of VB versus cutting time in different feed rates. The VB increases sharply with the increase of feed rate, and even the VB increases by about more than 60 μm at the cutting time of 15 min when feed rate

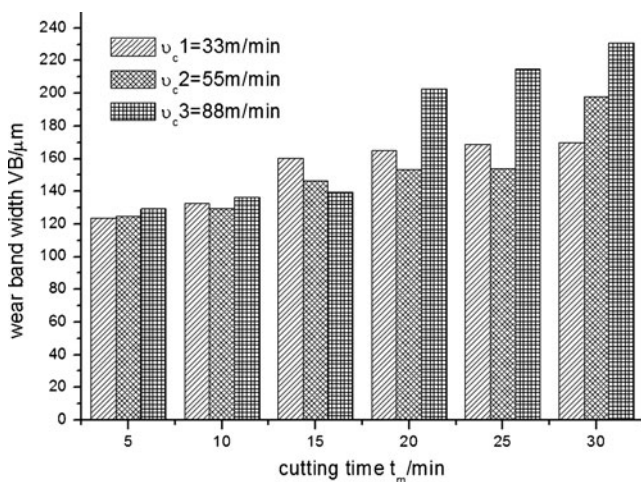


Fig. 9 Progression of VB versus cutting time under different cutting speeds (feed rate 0.1 mm/r, cutting depth 0.8 mm)

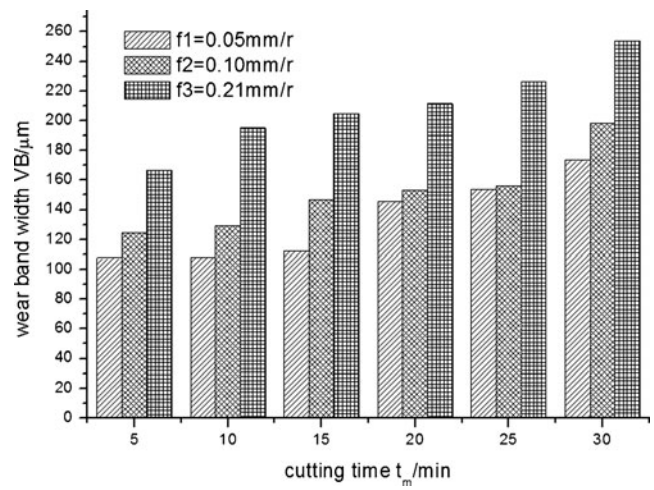


Fig. 10 Progression of VB versus cutting time under different feed rates (cutting speed 55 m/min, cutting depth 0.8 mm)

increases from 0.10 to 0.21 mm. The increase of feed rate extends the areas of the first and second shear deformation zones, and enlarges the removal per unit time. Consequently, it enhances the cutting temperature and the cutting force, intensifies the adhesive wear and diffusive wear, and finally reduces the tool life [10].

3.3.3 The influence of cutting depth

Figure 11 shows the progression of VB versus cutting time in different cutting depths; VB remains almost changeless with the cutting depth increasing. With the increase of the cutting depth, the cutting edge length participating in cutting also elongates. Although the cutting force and the cutting heat increase, the chip compression ratio and the average contact temperature remain unchanged [13]. Therefore, the cutting temperature and the wear rate basically remain changeless for the different cutting depths.

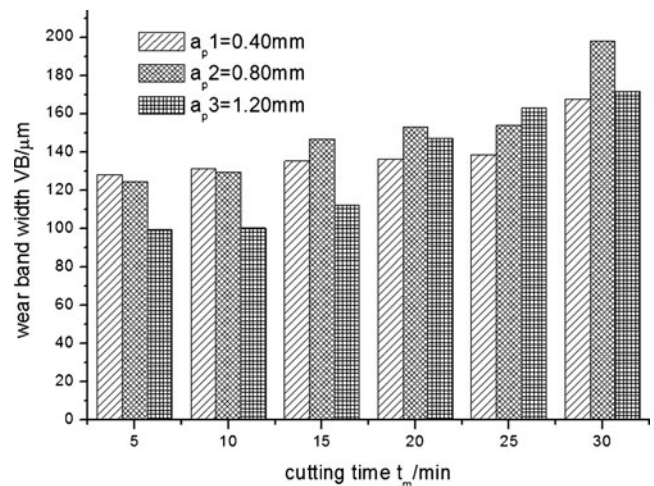
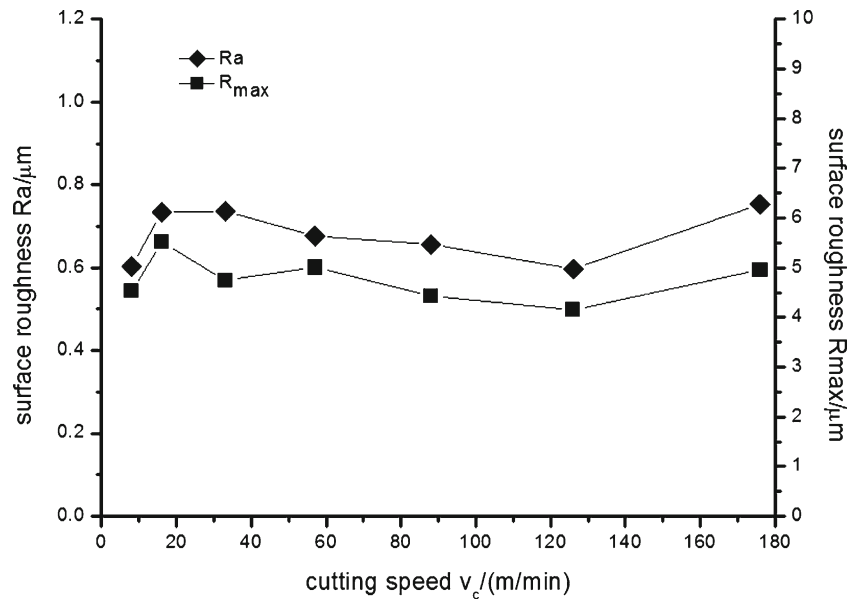


Fig. 11 Progression of VB versus cutting time under different cutting depths (cutting speed 55 m/min, feed rate 0.1 mm/r)

Fig. 12 Progression of surface roughness versus cutting speed (feed rate 0.1 mm/r, cutting depth 0.8 mm)



3.4 The influences of cutting parameters on surface roughness

3.4.1 The influence of cutting speed

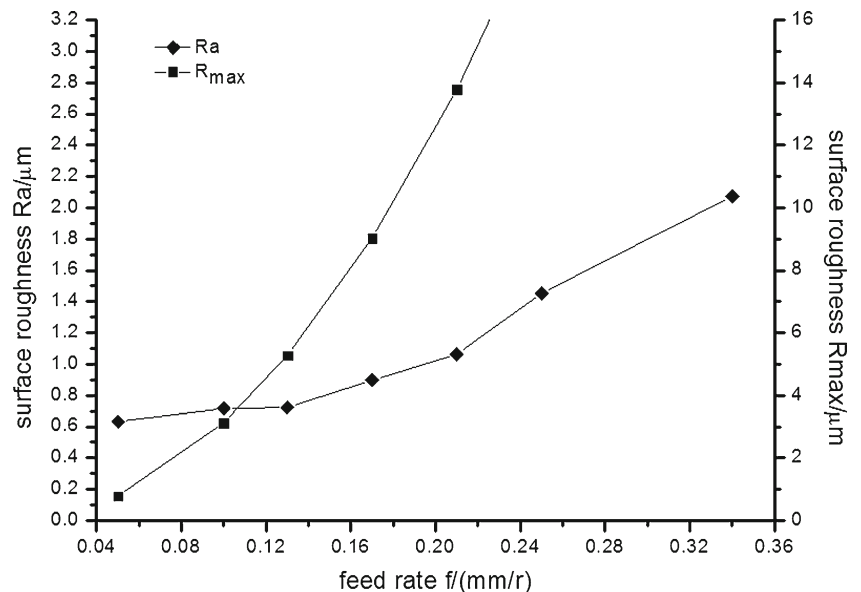
Figure 12 shows the progression of surface roughness versus cutting time at different cutting speeds. Obviously, the lowest surface roughness value is recorded at the low cutting speed. With the increase of cutting speed, the surface roughness value increases, and the highest surface roughness value is recorded at the cutting speed ranging from 16 to 33 m min⁻¹. This is probably due to the formation of built-up edge, which can induce the more severe vibration and scratch effect of the tool. Ramesh et al. [17] studied the relationship of surface roughness with cutting speed, and pointed out that built-up edge formation on cutting tool tends to develop bad surface

roughness. At the cutting speed ranging from 33 to 126 m min⁻¹, the forming condition of built-up edge is weakened gradually; the surface roughness decreases and tends to level off. The jumping phenomenon of the surface roughness values at the speed reaching to about 126 m min⁻¹ is probably caused by severe tool wear, after all the high cutting speed results in high cutting temperature and high cutting force.

3.4.2 The influence of feed rate

With the increase of feed rate, the surface roughness obviously and monotonically increases, as shown in Fig. 13. To the cutting tool with a circular blade, a basic theoretical model for surface roughness R_{max} is approximated by the following equation [18]:

Fig. 13 Progression of surface roughness versus feed rate (cutting speed 55 mm/min, cutting depth 0.8 mm)



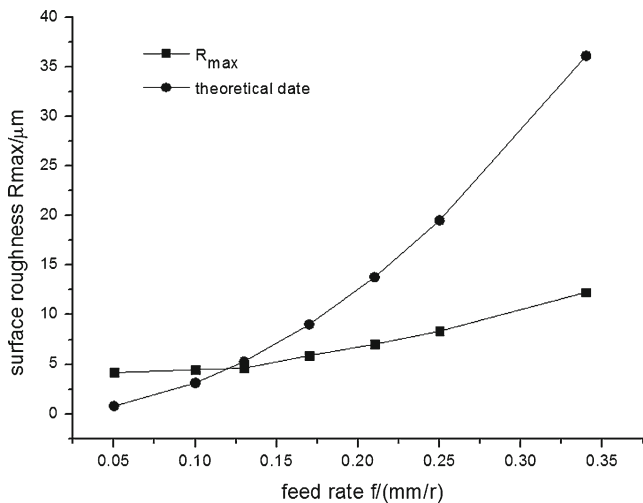


Fig. 14 Progression of experimental and theoretical surface roughness versus feed rate (cutting speed 55 m/min, cutting depth 0.8 mm)

$$R_{max} = \frac{f^2}{8r_\epsilon}$$

where f is feed rate (millimeters per rev.), and r_ϵ is the tool nose radius (in millimeters).

According to the theoretical model, the surface roughness is just related to feed rate and tool nose radius. However, the progressions of the experimental and theoretical dates versus cutting time at different feed rates shown in Fig. 14 present that the difference between the experimental and theoretical surface roughness is becoming bigger and bigger with the increase of feed rate. Meanwhile the variation tendencies are the same of the experimental and theoretical surface roughness versus feed rate. The increase of surface roughness with feed rate is attributed to the larger cutting force caused by

larger feed rate results in more violent vibration of machine-tool structure and worse surface roughness [18], and that the wear mechanism remains changeless and gradually aggravates with the increasing feed rate.

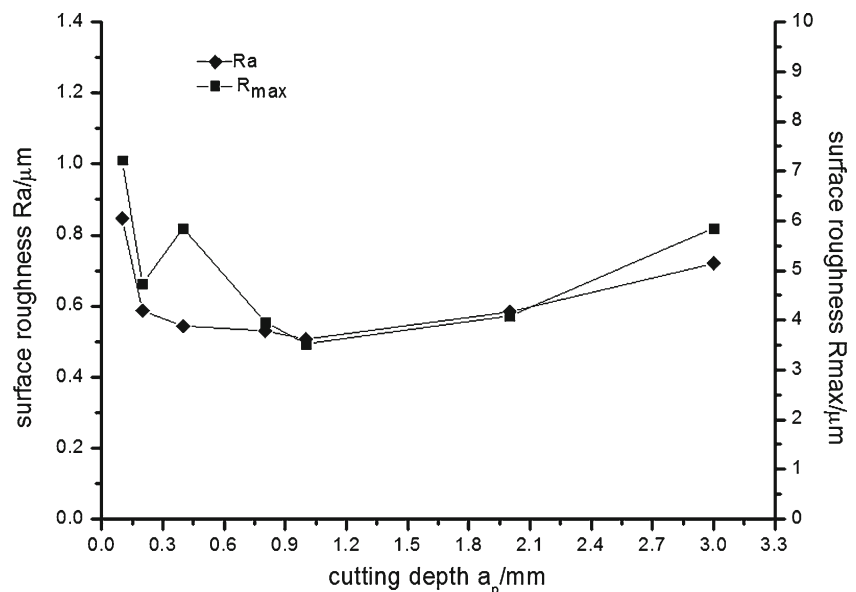
3.4.3 The influence of cutting depth on surface roughness

Figure 15 shows the progression of surface roughness versus cutting time for different cutting depths. The experimental curve has a minimum point when the cutting depth is about 1.0 mm. Generally, the influence of cutting depth is very small on cutting temperature, cutting force, and BUE. The appearance of the minimum point is caused by the nose radius of 0.4 mm. When the cutting depth is less than 0.4 mm, there exist three phenomena. Firstly, the cutting edge angle and the minor edge angle actually taking part in cutting are changed, because the tool nose tends not to fully take part in cutting. Secondly, the small contact area between the workpiece and the cutting tool decreases the amount of the heat generated. Thirdly, the heat transfer from the workpiece to the tool decreases, which tends to decrease the temperature of the workpiece and increase the temperature of the tool [19].

4 Conclusion

High-strength and wear-resistant aluminum bronze alloy was cut with the YW1 cemented carbide tool and YBC251 coated cemented carbide tool, respectively. The wear mechanisms of the two kinds of cutting tools and the influences of cutting parameters on the tool life and the surface roughness of YBC251 coated cemented carbide tool were analyzed. The conclusions can be drawn as follows:

Fig. 15 Progression of surface roughness versus cutting depth (cutting speed 55 m/min, feed rate 0.1 mm/r)



- The wear mechanisms of YW1 cemented carbide tool are adhesive wear, abrasive wear, and diffusive wear. The tool failure mode of the YW1 cemented carbide tool is micro-chipping.
- The wear mechanisms of YBC251 coated cemented carbide tool are adhesive and diffusive wear with slightly peeling wear and oxidative wear, and because of the coating failure and the adhesive wear, delaminating phenomenon appears in the cutting process. The machining performance of YBC251 tool is better than that of the YW1 tool, and even because of the appearance of the severe micro-chipping, the YW1 tool is not suitable to machine the aluminum bronze.
- The tool failure mode of YBC251 coating cemented carbide tool was the average flank wear. Under the actual working cutting condition, the tool life of the YBC251 coated cemented carbide tool is about 90 min.
- Due to the change of the main wear mechanisms of YBC251 coated cemented carbide tool with increase of cutting speed, the tool life and the surface roughness do not monotonically change with increasing cutting speed.
- From the influences of cutting parameters on the tool life and the surface roughness with YBC251 coated cemented carbide tool, feed rate has a stronger effect than cutting speed and cutting depth. And with the increase of feed rate, the tool life and surface roughness have a substantial decrease and increase, respectively.
- With the increase of cutting depth, the tool life of YBC251 coated cemented carbide tool remains basically constant, and the surface roughness has a minimum value at the cutting depth of 1.0 mm because of the nose radius.
- Prasad BK (2004) Sliding wear behavior of bronzes under varying material composition, microstructure and test conditions. *Wear* 257: 110–123
- Li WS, Wang ZP, Lu Y, Yuan LH, Xiao RZ, Zhao XD (2009) Corrosion and wear behaviors of Al-bronzes in 5.0% H_2SO_4 solution. *Trans Nonferrous Met Soc China* 19:311–318
- Tibballs JE, Erimescu R (2006) Corrosion of dental aluminium bronze in neutral saline and saline lactic acid. *Dent Mater* 22:793–798
- Li WS, Wang ZP, Lu Y, Gao Y, Xu JL (2006) Preparation, mechanical properties and wear behaviors of novel aluminum bronze for dies. *Trans Nonferrous Met Soc China* 16:607–612
- Wang L, Xu XL, Xu JJ, Hei ZK (2000) Microstructures and properties of PVD aluminum bronze coatings. *Thin Solid Films* 376:159–163
- Li YY, Ngai TL, Zhang DT, Xia W, Yan L (2000) Study on mechanisms of tool wear in turning a high strength wear resisting aluminum bronze. *Proceedings of the 4th International Conference on Frontiers of Design and Manufacturing, Shanghai, China*, pp. 351–355 (in Chinese)
- Li YY, Ngai TL, Xia W, Long Y, Zhang DT (2003) A study of aluminum bronze adhesion on tools during turning. *J Mater Process Technol* 138:479–483
- Da Silva RB, Vieira JM, Cardoso RN, Carvalho HC, Costa ES, Machado AR, De Àvila RF (2011) Tool wear analysis in milling of medium carbon steel with coated cemented carbide inserts using different machining lubrication/cooling systems. *Wear* 271:2459–2465
- Qi HS, Mills B (1996) On the formation mechanism of adherent layers on a cutting tool. *Wear* 198:192–196
- Niu QL, Chen M, Ming WW, An QL (2013) Evaluation of the performance of coated carbide tools in face milling TC6 alloy under dry condition. *Int J Adv Manuf Technol* 64:623–631
- Li AH, Zhao J, Luo HB, Pei ZQ (2012) Progressive tool failure in high-speed dry milling of Ti-6Al-4V alloy with coated carbide tools. *Int J Adv Manuf Technol* 58:465–478
- Nouari M, List G, Girot F, Géhin D (2005) Effect of machining parameters and coating on wear mechanisms in drilling of aluminium alloys. *Int J Mach Tools Manuf* 45:1436–1442
- Li R, Shih AJ (2006) Finite element modeling of 3D turning of titanium. *Int J Adv Manuf Technol* 29:253–261
- Wu Z, Deng JX, Chen Y, Xing YQ (2012) Performance of the self-lubricating textured tools. *Int J Adv Manuf Technol* 62:943–951
- Ramesh S, Karunamoorthy L, Palanikumar K (2012) Measurement and analysis of surface roughness in turning of aerospace titanium alloy (gr5). *Measurement* 45:1266–1276
- Cemal Cakir M, Ensarioglu C, Demirayak I (2009) Mathematical modeling of surface roughness for evaluating the effects of cutting parameters and coating material. *J Mater Process Technol* 209:102–109
- Mohamed NAN, Ng EG, Elbestawi MA (2007) Modelling the effects of tool-edge radius on residual stresses when orthogonal cutting AISI 316L. *Int J Mach Tools Manuf* 47:401–411

References

- Li YY, Ngai TL, Xia W (1996) Mechanical, friction and wear behaviors of a novel high-strength wear-resisting aluminum bronze. *Wear* 197:130–136
- Shi Z, Sun Y, Bloyce A, Bell T (1996) Unlubricated rolling-sliding wear mechanisms of complex aluminium bronze against steel. *Wear* 193:235–241